J. Chem. Thermodynamics 105 (2017) 352–361

Contents lists available at ScienceDirect

J. Chem. Thermodynamics

journal homepage: www.elsevier.com/locate/jct

Semifluorinated alkanes and alkanes: A phase study of the perfluorohexyloctane – Tetradecane system

Anna Runnsjö [a,b,*], Vitaly Kocherbitov [a,b], Gesche Graf [c], Anthony Pettigrew [c], Dieter Scherer [c], Kell Mortensen [d], Johan Engblom [a,b]

[a] Biomedical Science, Faculty of Health and Society, Malmö University, SE-205 06 Malmö, Sweden
[b] Biofilms – Research Center for Biointerfaces, Malmö University, SE-205 06 Malmö, Sweden
[c] Novaliq GmbH, Im Neuenheimer Feld 515, D-69120 Heidelberg, Germany
[d] Niels Bohr Institute, University of Copenhagen, Universitetsparken 5, 2100 København Ø, Denmark

ARTICLE INFO

Article history:
Received 6 November 2015
Received in revised form 3 October 2016
Accepted 21 October 2016
Available online 22 October 2016

Keywords:
Semifluorinated alkane
Perfluorohexyloctane
Tetradecane
Thermal phase behavior
Calorimetry
Small angle X-ray scattering

ABSTRACT

The binary system perfluorohexyloctane (F6H8)–tetradecane (C14) was investigated in order to increase understanding of interactions of semifluorinated alkanes (SFAs) with hydrophobic molecules. The thermal phase behavior for F6H8 and C14 and their mixtures was determined using DSC. The activity coefficients for both components in the mixtures were calculated and Gibbs energy of mixing was determined. Furthermore, enthalpies of mixing were determined with ITC and structural investigations of the solid and the liquid phases were performed with SAXS and SWAXD. It was found that F6H8 displays one solid-solid transition at −42.3 °C (ΔH = 1.1 kJ/mol) and one solid-liquid transition at −5.9 °C (ΔH = 16.6 kJ/mol). Due to the low enthalpy of the solid-liquid transition it is likely that F6H8 is not fully crystallized in the solid phase but partly amorphous. The F6H8–C14 system displays a eutectic phase behavior and the liquid mixtures display a positive deviation from ideal mixing. C14 crystalizes in a triclinic unit cell as shown before, whereas crystallization of F6H8 in a lamellar rippled phase is shown for the first time. This ripple phase comprises a bilayer of tilted alternating heavily interdigitated F6H8 molecules in an oblique subunit cell.

1. Introduction

Semifluorinated alkanes (SFAs) have, due to their special chemical and physical properties, been investigated in several studies. Composed of a hydrocarbon segment linked to one or two fluorocarbon segments they can generally be described by the formula $F(CF_2)n(CH_2)mH$, abbreviated as FnHm, for diblock structures and $F(CF_2)n(CH_2)m(CF_2)nF$ for triblock structures. SFAs display some interesting features being not only amphiphilic with fluorophilic and lipophilic regions, but also amphisteric and amphidynamic as the segments have different conformations and flexibility [1]. They are sometimes also referred to as primitive surfactants as some long chain SFA-molecules are able to spread on air/water interfaces forming a stable Langmuir monolayer [2,3], although none of the chain segments are hydrophilic.

Some SFAs can also form gels when dissolved in alkanes, perfluorinated fluids and liquid or supercritical CO_2 [4–7]. These viscous gel phases can be reversibly formed and are believed to be caused by encapsulation of solvent molecules between fibrous networks of lamellar SFA crystals [5,7–9].

One reason for the popularity of SFAs is their ability to form liquid crystals. Broniatowski et al. have used DSC and optical microscopy to confirm that perfluorooctyl-n-alkanes (F8Hm) form liquid crystals (smectic B phase) if the hydrogenated moiety comprises 8–11 carbon atoms [10]. Similarly, perfluorodecyl-n-alkanes (F10Hm) can form liquid crystals if the hydrogenated segment contains between 8 and 12 carbon atoms [3,11,12]. However, to the best of our knowledge no structural determination has previously been performed on the smaller F6H8, used in this study.

Due to the fact that SFAs are considered to be biologically stable [1], they have been considered for numerous pharmaceutical applications. For instance, SFAs have been considered for development of both pulmonary drug delivery vehicles [13] as well as for use in synthetic blood substitutes [14]. It has also been shown that

Abbreviations: C14, tetradecane; DSC, differential scanning calorimetry; F6H8, perfluorohexyloctane; ITC, isothermal titration calorimetry; SAXS, small angle X-ray scattering; SFAs, semifluorinated alkanes; SWAXD, small and wide angle X-ray diffraction.

* Corresponding author at: Biomedical Science, Faculty of Health and Society, Malmö University, SE-205 06 Malmö, Sweden.
E-mail address: anna.runnsjo@gmail.com (A. Runnsjö).

http://dx.doi.org/10.1016/j.jct.2016.10.032
0021-9614/

fluorocarbons and semifluorinated alkanes can be used to fluidize lung surfactants, providing a potential for usage in lung surfactant therapy [15]. Several studies exist where the possibility to use SFAs as eye tamponades to stabilize the retina during retinal surgery have been investigated, as SFAs with their good surface spreading properties and high density would be a good alternative to commonly used silicone oils [16–18]. Studies have also been performed to investigate the structure of SFA containing liposomes, for instance Schmutz et al. have shown that F6H10 molecules incorporate in between the hydrophobic part of the lipid bilayers, with the hydrogenated segment of the SFAs integrated between the lipid tails [19].

The SFA F6H8 also has a large potential for use against dry eye syndrome, as it can easily spread on and stabilize the tear film. The outermost layer of the tear fluid is an oily layer [20–23] and it is hence relevant to investigate how F6H8 interacts with hydrophobic components. In this study we have investigated the physicochemical interaction of F6H8 with tetradecane (C14), an alkene with the same chain length as F6H8. The thermal phase behavior was investigated using DSC and SWAXS/SWAXD, and isothermal titration calorimetry was used to determine enthalpy of mixing for F6H8 and C14.

2. Experimental

2.1. Chemicals

Perfluorohexyloctane (1,1,1,2,2,3,3,4,4,5,5,6,6-Tridecafluoro-tetradecane, purity > mole fraction 0.9988) was obtained from Novaliq GmbH (Heidelberg, Germany) while tetradecane (purity > mole fraction 0.99) was purchased from Sigma Aldrich. Properties of the substances used are given in Table S1.

2.2. Differential Scanning Calorimetry

Differential Scanning Calorimetry (DSC 1, Mettler Toledo, Greifensee, Switzerland) was used to characterize the phase behavior. DSC was employed to obtain data on transitions by temperature rising scans (heating rates = 0.2 C/min, 0.5 C/min and 1 °C/min). Extrapolation to a heating rate of 0 °C/min was used to determine endset temperatures while average from the three measurements were used to determine onset temperatures and enthalpy values of the transitions. Sealed standard aluminium crucibles (40 µl, Mettler Toledo) were used. Calibration for heat flow was done using indium (mp 156.6 °C; ΔH = 28.45 J/g). Onset of melting was used for calibration because it is almost independent on scan rate. To take into account the dependence of endset temperature with scan rate we used extrapolation to zero scan rate.

2.3. Isothermal titration calorimetry

Isothermal titration calorimetry (ITC) was performed on a 2277 Thermal activity Monitor (Thermometric). A sample volume of 3–4 ml was used and 8 consecutive injections of 10 µL/injection were added using a syringe pump (612 Lund Syringe Pump 2, Thermometric). The temperature was controlled to 25 °C during the measurements. Data treatment was performed in Matlab (MathWorks, Natick, Massachusetts, USA). Measured thermal powers were corrected with background subtraction and the Tian equation [24] with τ = 270 s for each injection and the heat for each injection was obtained by integration of the peaks.

2.4. Synchrotron small angle X-ray scattering (SAXS) measurements

Synchrotron SAXS measurements on F6H8 and C14 were performed at the MAX IV laboratory (Lund, Sweden). Measurements were performed at 25 °C on beamline 911-4, with a wavelength of 0.91 Å, a flux of 5 * 1010 photons/s, sample spot size of 0.3 × 0.3 mm^2, and a Pilatus 1M detector. Data reduction was done in the software Fit2D (Andy Hammersley, European Synchrotron Radiation Facility, Grenoble, France). Background subtraction was performed in Matlab. The same sample holder and capillary was used for data collection of background and sample. SasView (SasView, http://www.sasview.org/) originally developed by the DANSE project under NSF award DMR-0520547 was used to model the data.

2.5. Small and wide angle X-ray diffraction (SWAXD)

SWAXD measurements on F6H8 and C14 were performed using a Ganesha SAXS/WAXS instrument (SAXSLab/JJ-Xray, Denmark) with CuK_α-radiation (X-ray wavelength λ = 1.54 Å). The samples were mounted in sealed holders between two mica windows and measured in vacuum. The temperature of the sample holders was controlled from −50 °C to +25 °C using a Linkam LNP95 cooling system (Linkam Scientific Instruments Ltd., Tadworth, United Kingdom). Data analysis, including azimuthal averaging, was done using SAXSGui from SAXSLab.

3. Results and discussion

F6H8 is a semifluorinated alkane that has a large potential for several applications, among others treatment of dry eye syndrome. However, very little is known about its physicochemical properties. In order to increase the understanding of F6H8 interaction with hydrophobic molecules, we have made an in depth investigation of the phase behavior of F6H8–tetradecane (C14).

3.1. Thermotropic phase behavior for pure substances

Phase transitions of the pure components (C14 and F6H8) were investigated using differential scanning calorimetry (DSC). Fig. 1 displays DSC scans with a heating rate of 1 °C/min for C14 (A) and F6H8 (B). C14 displays one solid-liquid transition point with onset at 5.9 ± 0.6 °C and an enthalpy of 242 ± 4 J/g corresponding to 48.0 ± 0.8 kJ/mol, where standard uncertainties are given as errors. The measured melting temperature is in agreement with previous studies which report a melting temperature between 5.3 °C and 6.8 °C [25–29]. Our measurements gave however a slightly higher value of the melting enthalpy of C14 compared to previous studies which report 45 kJ/mol [30–32] and sometimes as low as 38 kJ/mol [33]. This slightly higher enthalpy value could be due to the fact that the DSC was calibrated with Indium which has a rather high melting temperature (156.6 °C) compared to tetradecane (5.9 °C), which may cause a small error in the enthalpy measurement.

Pure F6H8 displays two endothermic transitions with onsets at −42.3 ± 0.8 °C and −5.9 ± 0.6 °C, and enthalpies of 2.7 ± 0.7 J/g and 38.5 ± 0.3 J/g corresponding to 1.1 ± 0.3 and 16.6 ± 0.6 kJ/mol respectively. The standard uncertainties are given as the errors. The solid-liquid transition at −5.9 °C has a smaller melting enthalpy than expected (37.7 kJ/mol) and the reason for this is partial crystallinity of F6H8, which will be discussed below. The minor transition at −42.3 °C has a non-sharp onset as can be seen in the insert of Fig. 1B. Furthermore, a dependence was found between the scan rate and the enthalpy of the peak, with highest enthalpy obtained with the lowest scan rate. This indicates that it is a non-equilibrium transition with strong kinetic effects. This can also be observed in X-ray measurements where differences between measurements performed at −14 °C and −46 °C are only occasionally seen. The non-sharp onset could be an indication of

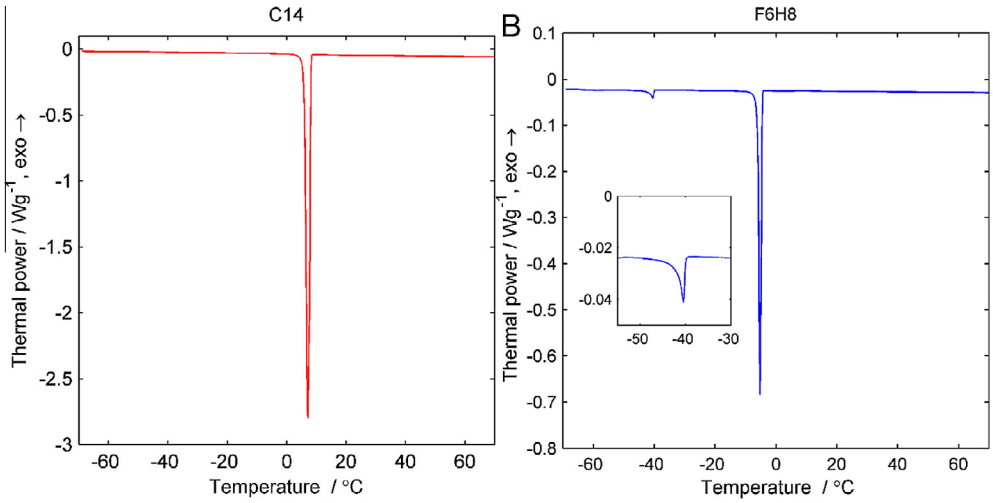

Fig. 1. Thermotropic phase behavior for C14 and F6H8. C14 (A) displays one solid-liquid phase transition with onset temperature at 5.9 °C while F6H8 (B) displays two phase transitions with onset temperatures of −42.3 °C (solid-solid) and −5.9 °C (solid-liquid). The insert in B displays the smaller peak in F6H8 at −42.3 °C. DSC measurements with a heating rate of 1 °C/min are shown.

low purity samples, however as samples with high purity (mole fraction 0.9988) are used in this study, impurities are not likely to be the reason for the occurrence of this peak. Neither can this peak be assigned to a solid-liquid transition due to the low enthalpy value of 1.1 kJ/mol. Minor transition points, in addition to the main transition, are also observed in other SFAs. The appearance of these minor transitions is dependent on the chain length of the fluorinated and hydrogenated segments [3,6,10–12,34,35]. The nature of these transitions have previously been assigned to transitions between two liquid crystalline structures [3,10], crystal and liquid crystal structures [3,10], or increased mobility of the molecules [11,36].

The main transition point of F6H8 at −5.9 °C is in agreement with the previous reported melting point of F6H8 at −5.2 °C [37,38]. To assess the origin this transition point in F6H8 at −5.9 °C, the obtained enthalpy value (16.6 kJ/mol) was compared with literature values for perfluorocarbons and n-alkanes of various chain lengths. The melting enthalpy for both perfluorocarbons and n-alkanes displayed a linear dependence with number of carbon atoms in the molecules [30,39–41], Fig. 2.

From a linear fit to literature data for fluorocarbons and n-alkanes a predicted enthalpy of melting for the fluorinated and hydrogenated segment in F6H8 was calculated as described in equation 1:

$$\Delta H_p = 6 * \Delta H_F + \Delta H_{F-end} + 8 * \Delta H_H + \Delta H_{H-end} \quad (1)$$

were ΔH_p is the predicted value, ΔH_F and ΔH_H is the enthalpy per carbon in fluorocarbons and n-alkanes, respectively, calculated as the slope in Fig. 2. The $\Delta H_{F\text{-}end}$ and $\Delta H_{H\text{-}end}$ terms are added in order to consider the contributions from terminal carbons in the fluorinated and hydrogenated segment, respectively. They are calculated as half the y-intercept in Fig. 2. Using this model we predicted enthalpy of melting for F6H8 to 37.7 kJ/mol, which is much larger than the measured value of 16.6 kJ/mol. It is therefore not likely that a solid-liquid transition of both the hydrogenated and fluorinated segment occurs at this transition point. Instead either the fluorinated or hydrogenated part melts during this transition. Our model predicts that melting of the hydrogenated segment in F6H8 would give an enthalpy value of 24.6 kJ/mol while melting of the fluorinated segment would correspond to an enthalpy of 13.1 kJ/mol. Thereby our model suggest that melting of the fluorinated segment occur in the main transition point of F6H8, as this gives the closest value to the measured enthalpy of 16.6 kJ/mol.

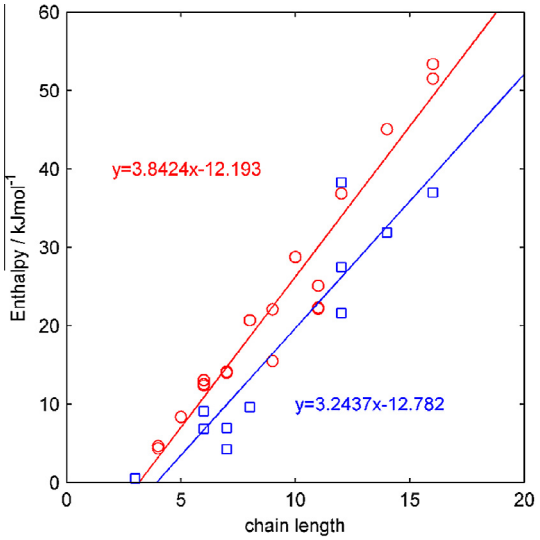

Fig. 2. Enthalpy of melting for n-alkanes (red circles) and perfluorocarbons (blue squares) obtained from literature [30,39–41]. A linear increase is seen with number of carbons in the chain. (For interpretation of the references to colour in this figure legend, the reader is referred to the web version of this article.)

Several studies have previously found that the melting energies for both F12Hm [11,35] and F10Hm [3,11] are significantly lower compared to perfluoroalkanes and alkanes of similar chain length. Furthermore, for small to medium length of the hydrogenated segments no increase in the melting energies were found. A linear dependence with hydrogenated segment length was found for m > 12 in the case of F12Hm and m > 16 in the case of F10Hm [10,11,35]. In addition, the melting temperature is strongly dependent on the length of the fluorinated segment [36]. Combining the temperature dependence on fluorinated segment length with increase in melting energy due to increased length of the hydrogenated segment Fujiwara et al. [11] concluded that disordering of the complete molecule is involved in the melting of SFA molecules. However due to the low melting energy F6H8 has to be partly disordered also below the melting temperature. Raman as well as solid state 13C NMR studies have shown that at least the hydrocarbon segments in several SFAs are in a liquid like conformation and isolated from adjacent hydrocarbon chains below the

melting temperature [6,36]. This is in good agreement with our conclusion that the hydrogenated segment of F6H8 remains disordered below the melting temperature while the fluorinated segment crystalizes [36].

3.2. Thermotropic phase behavior for F6H8–C14 mixtures

In order to obtain information on changes of thermotropic phase behavior in F6H8:C14 mixtures, DSC measurements were performed for a series of mixing ratios, see Tables S2–S4. Thereby the phase diagram displayed in Fig. 3 could be obtained. F6H8 and C14 display a eutectic phase behavior with a eutectic point at a weight fraction of 0.04 C14 as determined from the intersection of the two liquidus lines. The eutectic temperature is −8.8 °C as determined by the average onset of the melting.

Transition points for the liquidus transitions (triangles) were obtained from endset of the transitions where a linear dependence with the heating rate exists (Supporting information Fig. S1). Extrapolation to a scan rate of 0 °C/min was performed to obtain close to equilibrium values for the liquidus line using data obtained with heating rates of 1 °C/min, 0.5 °C/min and 0.2 °C/min. The eutectic line (squares) and the low temperature phase transition for F6H8 (circles) were calculated as average of the onset temperature for all heating rates, as no dependence with the heating rate is observed in this case (Supporting information Fig. S1). The fit to the liquidus line was obtained from the Schröder equation and four-suffix Margules equation as described in Section 3.3, while the fit to the eutectic and low temperature lines were obtained as average of the measured points.

3.3. Activity coefficients from the phase diagram

F6H8–C14 mixtures display a eutectic phase behavior as seen in Figure 3. The Schröder equation (Eq. (2)) [42] describes the course of liquidus in simple eutectic systems. The original equation featured the concentration but for strict thermodynamic considerations the equation is modified to involve activity instead of concentration.

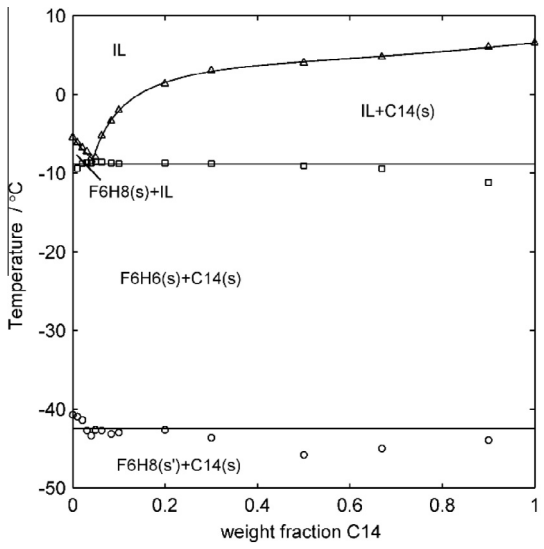

Fig. 3. Binary phase diagram of F6H8–C14 with a eutectic point of −8.8 °C at a weight fraction of 0.04 C14. Above the liquidus line, an isotropic liquid (IL) exists, between the eutectic and liquidus line isotropic liquid coexist with solid F6H8 (F6H8(s)) or solid C14 (C14(s)) and below the eutectic line solid F6H8 is in coexistence with solid C14. At −43 °C F6H8 undergoes a solid-solid transition: the low-temperature phase is denoted as s'.

$$\ln(a_i) = \frac{\Delta H_{melt}}{R} 1 \tag{2}$$

$$a_i = x_i \cdot \gamma_i \tag{3}$$

where a_i is the activity of component i (in this case F6H8 or C14), γ_i is the activity coefficient of component i, ΔH_{melt} and T_0 is the heat effect and melting temperature of pure component i, while T is the melting temperature of the mixture. The modification of the Schröder equation to involve activity instead of concentration allowed us to calculate the activities for F6H8 and C14 on the left and right side of the eutectic point, respectively. Deviation between the onset and extrapolated endset temperatures were found for the mixtures but also for the pure substances. This could be due to impurities in the system or surface effects caused by finite domain size. Therefore extrapolated endset temperatures were used for calculations of the activities for both the mixtures and the pure substances. Furthermore, in order to ensure the accuracy in our calculations we investigated whether C14 and F6H8 form solid solutions, as discussed later in Section 3.6. The calculated activities can be seen in Fig. 4A and corresponding activity coefficients are displayed as the points in Fig. 4B. The C14–F6H8 system displays a positive deviation form ideal mixing. Hence the solids are expected to be stable at higher temperatures compared to ideal mixing.

The activities of F6H8 and C14, Fig. 4A, were calculated using the Gibbs-Duhem equation (Eq. (4)) which can be used to obtain the activities of both components for any given binary mixture [43].

$$x_1 \mathrm{d}\ln(a_1) + x_2 \mathrm{d}\ln(a_2) = 0 \tag{4}$$

Before utilizing the Gibbs-Duhem equation (Eq. (4)) the activity coefficients of C14 were fitted to four-suffix Margules equation (Eq. (5)) [43], red line in Fig. 4B.

$$\ln(\gamma_1) = \alpha_2 x_2^2 + \alpha_3 x_2^3 + \alpha_4 x_2^4 \tag{5}$$

where, α_2, α_3 and α_4 are fitting parameters found to be 2.70, −2.76 and 1.59, respectively. According to Prausnitz et al. [43] combining the Gibbs-Duhem equation with the four-suffix Margules equation gives

$$\ln(\gamma_2) = \left(\alpha_2 + \frac{3}{2}\alpha_3 + 2\alpha_4\right)x_1^2 - \left(\alpha_3 + \frac{8}{3}\alpha_4\right)x_1^3 + \alpha_4 x_1^4 \tag{6}$$

Utilizing Eq. (6) the activity coefficient for F6H8 was obtained and is displayed as the blue line in Fig. 4B. As seen a good agreement exists between the activity calculated from the Schröder (blue stars) and Gibbs-Duhem equation. As the eutectic point is at high mole fraction of F6H8 (0.90) and the activity coefficient for F6H8 at this high concentration of F6H8 is very close to one, calculation of the activity coefficients for C14 from the activity coefficients of F6H8 will give rise to large errors and was hence not preformed.

Using the four-suffix Margules equation we could also obtain a good fit for the liquidus line on both the C14 and F6H8 side of the eutectic point in the phase diagram, Fig. 5A.

Furthermore, using the equations

$$G^{mix} = RTx_1\ln(a_1) + RTx_2\ln(a_2) \tag{7}$$

$$G^{E} = RTx_1\ln(\gamma_1) + RTx_2\ln(\gamma_2) \tag{8}$$

We calculated Gibbs energy of mixing, G_{mix}, (dashed line in Fig. 5B) and the Gibbs excess energy, G_E, (solid line in Fig. 5B). As can be seen the excess energy is positive for all mole fractions showing a positive derivation form ideal mixing. Furthermore the free energy is found to be unsymmetrical with respect to the mole fraction of the components.

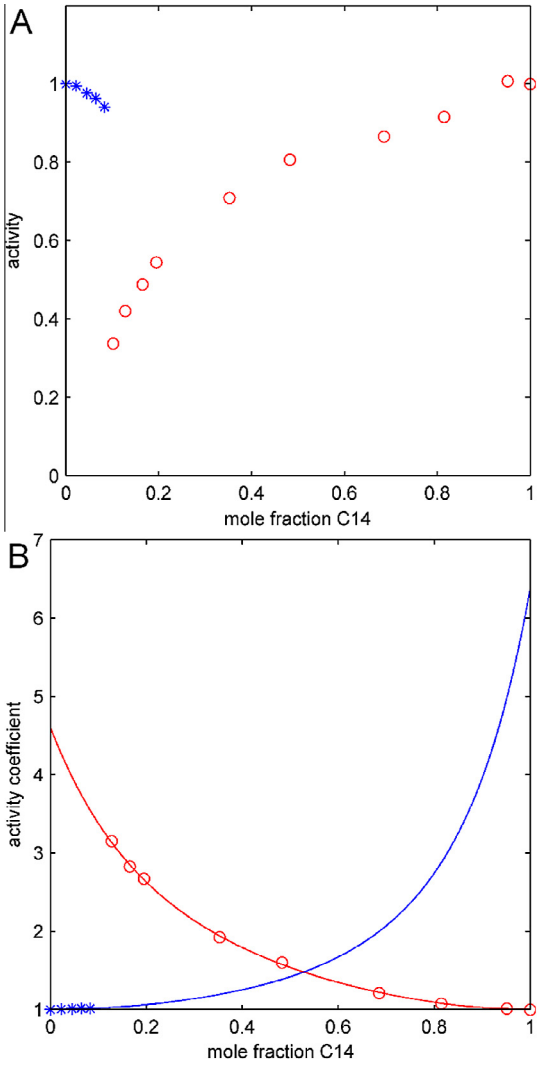

Fig. 4. Activities (A) and activity coefficients (B) for F6H8 and C14 as function of the mole fraction C14 in the sample. Activity and activity coefficient calculated from the Schröder equation (Eq. (2)) for F6H8 and C14 are displayed as blue stars and red circles, respectively. Four-suffix Margules equation (Eq. (5)) was used to fit the activity coefficient for C14 (red lines) and combined with Gibbbs-Duhem equation used to obtain the activity coefficient for F6H8 (blue line). (For interpretation of the references to colour in this figure legend, the reader is referred to the web version of this article.)

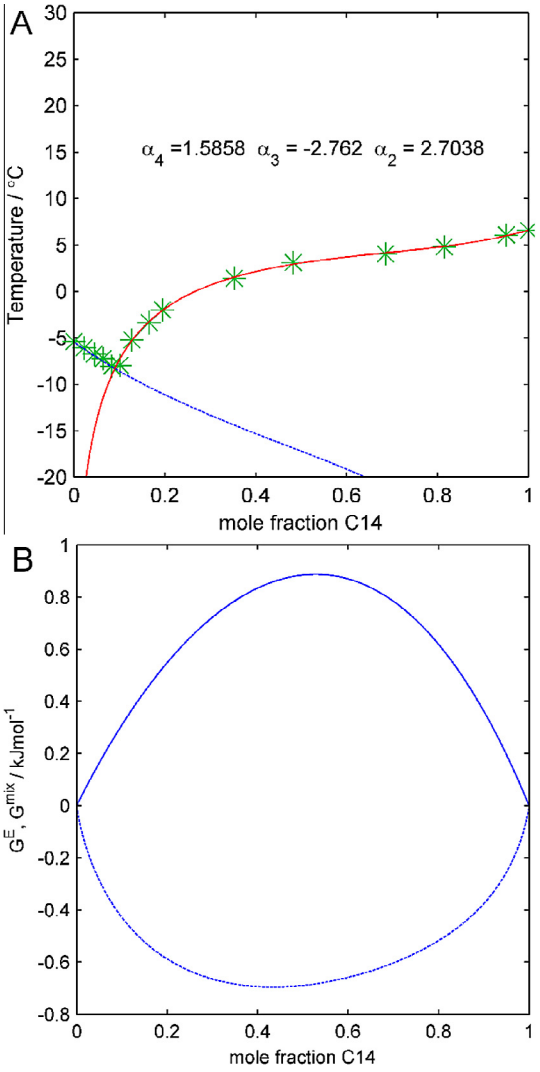

Fig. 5. A) Application of Schröder equation (Eq. (2)) combined with four-suffix Margules equation (Eq. (5)) could be used to obtain a good fit to predict the liquidus lines for F6H8–C14 mixtures. B) Gibbs energy of mixing (dashed line) and Gibbs excess energy (solid line) calculated from the activity coefficient of F6H8 and C14 obtained using four-suffix Margules equation.

3.4. Enthalpy of mixing for F6H8–C14

The partial molar enthalpy of mixing for F6H8 and C14 was investigated using isothermal titration calorimetry (ITC). Fig. 6 displays titration of C14 into F6H8 and titration of F6H8 into C14, the measured values are reported in Tables S5 and S6. Fig. 6A shows the obtained thermal power from injection of C14 and Fig. 6B displays calculated heat. In Fig. 6C the obtained thermal power for titration of F6H8 into C14 is shown while the calculated heat is displayed in Fig. 6D. To accurately determine the heat obtained for addition of C14 into an infinite amount of F6H8, the linear regime in Fig. 6B and D was used to extrapolate to zeroth injections and obtain enthalpy of solution at infinite dilution, $\Delta_{sol}H^{\infty}$. Titration of C14 to F6H8 results in an endothermic reaction with $\Delta_{sol}H^{\infty}$(C14) of 4.5 kJ/mol. Titration of F6H8 into C14 also give rise to large endothermic energy with $\Delta_{sol}H^{\infty}$*(F6H8)* of 6.5 kJ/mol. The larger value for $\Delta_{sol}H^{\infty}$*(F6H8)* compared to $\Delta_{sol}H^{\infty}$*(C14)* is again an indication of that the system is asymmetric, as can be seen in the calculated activity coefficient (Fig. 4B) and unsymmetrical Gibbs energy (Fig. 5B).

3.5. Fluid phase structural investigation

Structural investigation of the fluids at room temperature was performed using synchrotron SAXS. Measurements were performed on F6H8, C14 and 90:10 and 10:90 w/w mixtures of F6H8–C14 at the MAX IV laboratory (Lund, Sweden). F6H8 exhibits one broad peak at q 3.75 nm^{-1} (d-spacing of 1.68 nm), Fig. 7. The appearance of this peak indicates that F6H8 has a local structuring due to self-assembly. The d-spacing is close to the size of a distorted F6H8 molecule, which suggests local separation of fluorinated and hydrogenated parts in this isotropic fluid. This is in agreement with our MD simulations, which will be presented separately. Swelling of the aggregates are observed upon dilution with C14 and in a 90:10 mixture of F6H8:C14 the peak has shifted to lower q, corresponding to a d-spacing of 2.09 nm. Upon further dilution the local organization disappears and samples with 90% C14 and above do not display any clear peaks in the SAXS spectra.

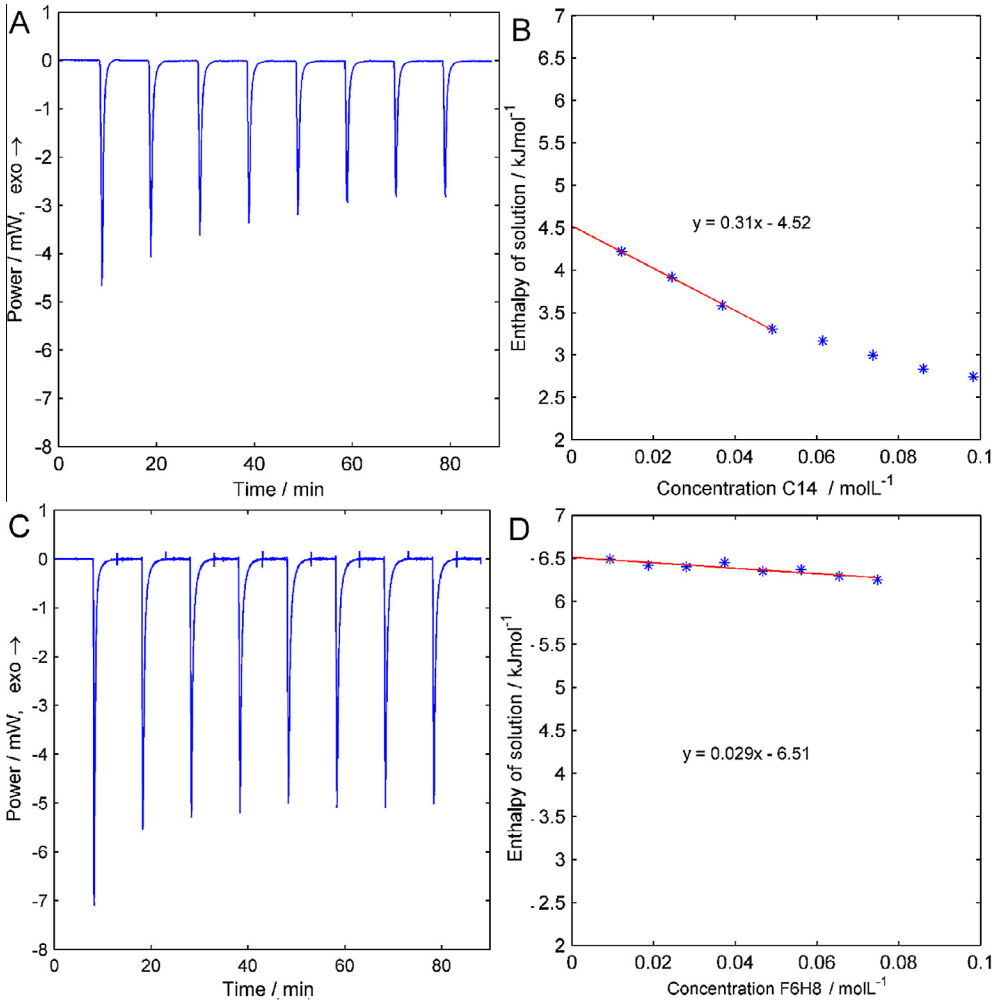

Fig. 6. Isothermal titration calorimetry (ITC) for titration of C14 into F6H8 and F6H8 into C14. A) Thermal power for titration of C14 into 3.1 mL of F6H8. B) Acquired enthalpy in each injection obtained by integration of the peaks in A). C) Thermal power for titration of F6H8 into 3.5 mL of C14. D) Acquired enthalpy in each injection obtained by integration of the peaks in C). In each injection 10 μL were injected and the curves in A and C are corrected by baseline subtraction and Tian equation with τ = 270 s. The linear regime corresponding to the four first injections in B and all 8 injections in D were used for extrapolation to zeroth injection. Concentration of F6H8 and C14 were calculated using densities of 1.331 g/mL for F6H8 and 0.762 g/mL for C14.

For the diluted sample with 0.1 wt fraction of F6H8 where the local ordering is gone, further analysis of the individual SFA molecules was performed by data modelling in the software SasView. The background corresponding to a capillary containing C14 was subtracted before modelling. A model for oriented cylinders described by Eqs. (9) and (10) [44] was used to fit the data.

$$P(q,\alpha) = \frac{scale}{V}\int_0^{\pi/2} f^2(q,\alpha)\sin\ \alpha\, d\alpha + bkg \tag{9}$$

$$f(q,\alpha) = 2(\Delta\rho)V\frac{\sin\ qL\ \cos\ \alpha/2}{qL\ \cos\ \alpha/2}\frac{J_1(qr\ \sin\ \alpha)}{qr\ \sin\ \alpha} \tag{10}$$

where $P(q,\alpha)$ is the 2D scattering intensity, α is the angle between the axis of the cylinder and the q-vector, V is the volume of the cylinder, L is the length of the cylinder, r is the radius of the cylinder, $\Delta\rho$ is the scattering length density difference between the scatterer and the solvent taken as an arbitrary value in our modelling, J_1 is the first order Bessel function and bkg is the background. It was found that cylinders with a radius of 0.3 nm and a length of 1.9 nm gave the best fit to our data, Fig. 8. This is slightly less than the length of the full molecule (2.1 nm) but longer than the length of the fluorinated segment (0.9 nm), which is the part that gives rise to contrast in the scattering to the bulk of C14. Other models such as spherical and elliptical shapes were also evaluated but no good fit was found using these models.

As a relatively high concentration (10 wt%) of SFA molecules was used we included a structure factor in the modelling to account for potential interactions between molecules or aggregates. The hard sphere structure factor, which does not implicate micelle formation but instead describes excluded volume interactions, was found to give the best with our data, Fig. 8. In this model the volume fraction of fluorinated segments was fixed to 0.0335, calculated from the mass fraction of F6H8 and the densities for perfluorocarbons and n-alkanes.

3.6. Solid state structural investigations

In addition to investigating fluid F6H8, C14 and mixtures thereof at room temperature, structural investigations were also performed using SWAXD at temperatures below the eutectic line, −8.5 °C. Pure C14 displayed a diffraction pattern corresponding to a fully crystalline material at −14 °C (Fig. 9) and we confirmed previous reports that tetradecane crystallize in a triclinic lattice [45,46]. Lattice parameters are shown in Table 1.

F6H8 also generates a set of Bragg peaks corresponding to an ordered crystalline structure at temperatures below the melting

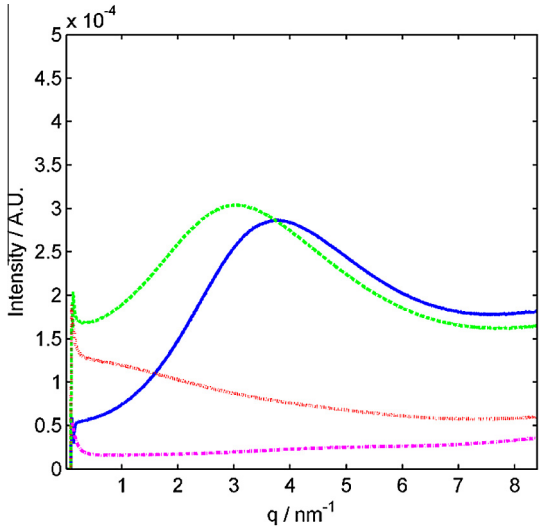

Fig. 7. Small angle X-ray scattering (SAXS) measured for F6H8, C14 and mixtures thereof. The samples contained 1 (blue solid line), 0.9 (green dashed line), 0.1 (red dotted line) and 0 (magenta dash-dot line) weigh fraction of F6H8. Background acquired with empty capillary is subtracted for all samples. (For interpretation of the references to colour in this figure legend, the reader is referred to the web version of this article.)

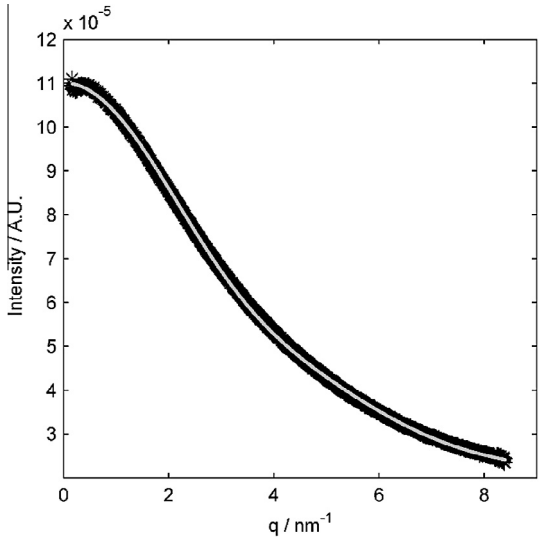

Figure 8. SAXS profile for a C14 sample containing F6H8 at a weight fraction of 0.1. Background corresponding to the capillary containing pure C14 was subtracted. Experimental data (black stars) as well as the best obtained fit (grey dots), using the monodisperse cylindrical model with a radius of 0.3 nm, a length of 1.9 nm and a hard sphere structure factor is shown.

temperature, −5.9 °C (Fig. 10). However, the diffractogram contains an additional diffuse "peak" with a maximum close to $q = 4\ nm^{-1}$, similar to the spectrum for liquid F6H8 at room temperature shown in Fig. 7. This is in agreement with the DSC measurements where we found that the enthalpy change for the main transition in F6H8 was smaller than expected from melting of a fully crystalline sample. It corresponds to what is expected for melting roughly half the F6H8 molecule and it is likely that the fluorinated or hydrogenated segment remains amorphous at −14 °C. Indeed, several studies on SFAs have shown that the hydrogenated segments do not close pack [6] and have a liquid like conformational freedom below the melting transition [36].

A closer look at the WAXD-part of the diffractogram (Fig. 10) allows us to deduce the sub-unit cell packing of the F6H8 molecules. It has previously been suggested that SFA crystals orient in a hexagonal rotator phase similar to odd n-alkanes [6,35,47]. A hexagonal structure would however only give rise to one peak while our measurements at -14 °C give rise to three peaks at $q = 13.66$, 13.84 and $14.66\ nm^{-1}$ (Fig. 10). These peaks best describe an oblique (monoclinic 2D) sub cell with lattice parameters a and c equal to 0.86 and 0.54 nm, and the corresponding angle β 91.1° (i.e. close to a rectangular (orthorhombic 2D) lattice, $\beta = 90.0°$) (Table 2, Fig. 11) [48]. The difference in peak intensities is furthermore somewhat problematic since $\beta = 91.1°$ is close to orthogonal we therefore would expect similar intensities in the (1_1) and (−1_1) peaks. It is possible to index these Bragg peaks as corresponding to two coexisting subunit cells and the higher intensity in the (−1_1) peak can then result from a coexisting hexagonal phase (indexed on a rectangular lattice, a = 0.92 nm, c = 0.53 nm and β = 90). Two coexisting subunit cells may perhaps favour formation of the ripple phase proposed below, but no additional peaks at higher q's related to a hexagonal phase could be observed in the provided diffractogram (Fig. 10 and 0 < q < 30+).

It is furthermore interesting to note that while hydrocarbons may crystallize in a hexagonal or orthorhombic sub cell with $q_{110} \approx 15\ nm^{-1}$ [49], fluorocarbons (like F20H0) and SFAs (like F12H8) give $q_{110} \approx 13\ nm^{-1}$ for the hexagonal sub cell [6,47]. This evidences the larger cross-sectional area displayed by fluorinated carbon chains compared to hydrogenated ones. Relating these facts to our partly fluorinated F6H8 with a monoclinic sub cell and $q_{11} \approx 14\ nm^{-1}$ (Table 2) we conclude that its cross-sectional area is close to the average of what would be expected for a pure hydrocarbon and a pure fluorocarbon crystal, respectively. Therefore, the F6H8 crystal has to comprise an alternating.

The SAXD-part of the diffractogram (q-range $1–13\ nm^{-1}$, Fig. 10) reveals a rather complex set of eight Bragg peaks at −14 °C (Table 3). Four of these peaks, related to the first and most intense peak ($q = 3.10\ nm^{-1}$), meet the higher order condition for a lamellar phase with a layer spacing of 2.03 nm. However, such simple lamellar structure does not accommodate the remaining four Bragg peaks. Instead we observe the similarity between our diffractogram (Fig. 10) and the one presented by Marczuk and Lang for F12H8 [47], from which they propose an undulating lamellar ripple phase based on a two-dimensional oblique unit cell. Indeed it is also possible to index our SAXD pattern in this way (Table 3) based on equation 11:

$$q_{h,k} = \frac{2\pi}{sin\Gamma}\sqrt{\frac{h^2}{A^2} + \frac{k^2}{B^2} - \frac{2hk}{AB}cos\Gamma} \qquad (11)$$

We propose that F6H8 also crystallizes in a lamellar ripple phase which is illustrated in Fig. 11. The lattice parameters A, B and Γ for this ripple phase at −14 °C are 9.42 nm, 4.64 nm and 167.6°, respectively, where the ripple wave length, λ, is reflected in A (Table 3). The F6H8 molecules form a tilted alternating monolayer structure with an oblique subunit cell. The density (ρ) corresponds to $1.558\ g/cm^3$, which is slightly lower than expected from a fully crystalline system but higher than what would be obtained with liquid like hydrocarbon parts ($1.331\ g/cm^3$). Based on the estimated length of one single F6H8 molecule (2.1 nm) the tilting angle, ψ, has to be approximately 18.4°. Capital letters are used to distinguish the lattice parameters for the ripple phase from those describing the sub-cell. To our knowledge this is the first time such rippled phase has been identified for SFA's above their minor transition point (c.f. F6H8: −42 °C, Figure 3).

Attempts were also made to resolve the structure of F6H8 below the minor transition point, -42 °C. At −46 °C only a small change in the diffraction pattern for F6H8 was seen compared to

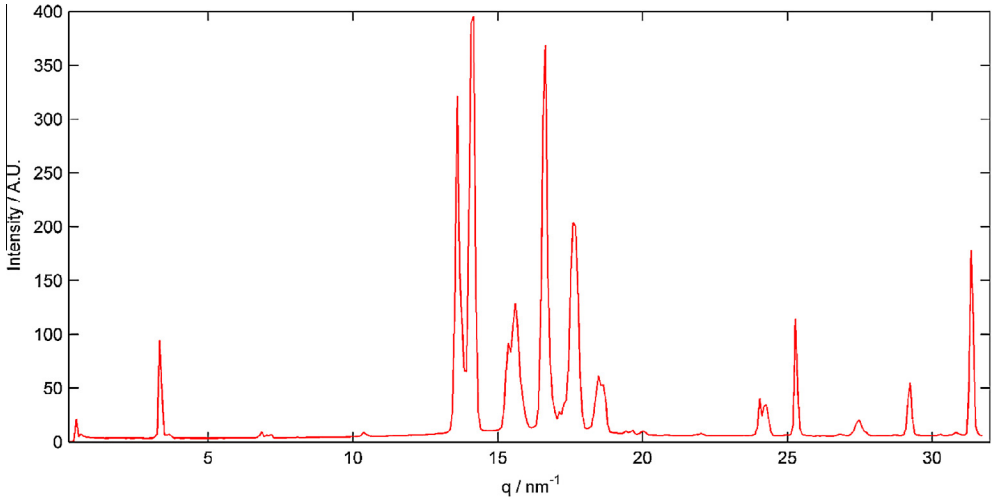

Figure 9. X-ray diffractogram of tetradecane at -14 °C. packing of hydrogenated and fluorinated carbon segments to fit the structural requirements.

Table 1
Lattice parameters (a, b, c, α, β, γ) and densities (ρ) for triclinic C14 crystals obtained in our study and in the previous study by Nyburg et al. [45] at pressure (P) of 0.1 MPa[a].

	a/nm	*b*/nm	*c*/nm	*α*/°	*β*/°	*γ*/°	*ρ*/g cm^{-3}	*T*/°C
Current study	0.429	0.481	2.00	84.54	65.99	73.61	0.915	−14
Nyburg et al. [45]	0.429	0.482	1.98	84.10	66.82	73.00	0.920	Not specified

[a] Standard uncertainties u in the current study are u(ρ) = 0.052 g cm^{-3}, u(T) = 1 °C and u(P) = 0.03 MPa.

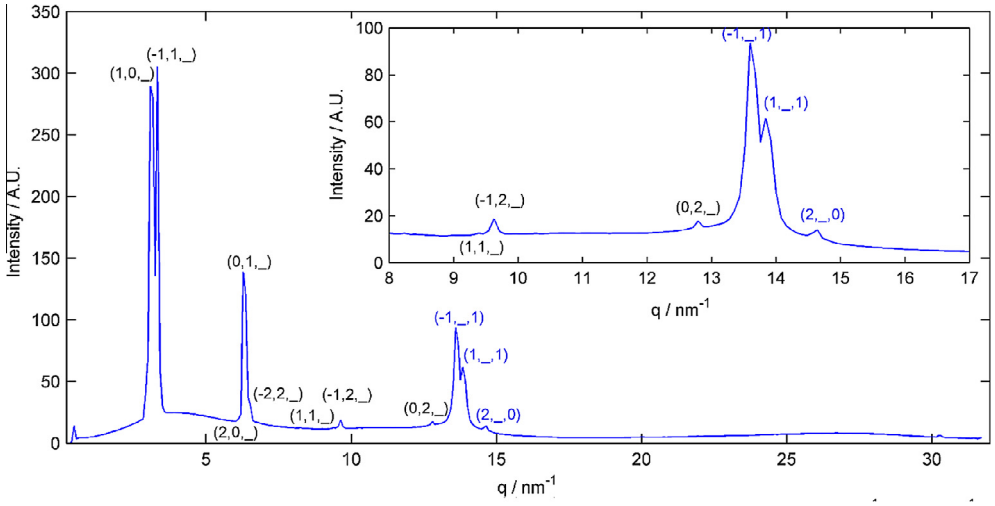

Figure 10. X-ray diffractogram of F6H8 at −14 °C. The insert displays a magnification from q = 8 nm^{-1} to 17 nm^{-1}. (*h*,_,*l*) values are assigned in blue to peaks used for calculation of the monoclinic subunit cell and (*h*,*k*,_) values are assigned in black to peaks originating from the ripple phase structure. (For interpretation of the references to colour in this figure legend, the reader is referred to the web version of this article.)

Table 2
Observed and calculated peak positions (***q*$_{Obs}$** and ***q*$_{Calc}$**) together with corresponding lattice parameters (a, c and β) and miller indexes (h, k, l) for the monoclinic sub-cell of the F6H8 crystal measured at two temperatures (T), −14 °C and −46 °C, respectively at pressure (P) of 0.1 MPa[a].

T/°C	*h*	*k*	*l*	q_{Obs}/nm^{-1}	q_{Calc}/nm^{-1}	Δq/nm^{-1}	*a*/nm	*c*/nm	*β*/°
−14	−1	_	1	13.60	13.60	0.002	0.86	0.54	91.13
	1	_	1	13.84	13.84	0.002			
	2	_	0	14.66	14.66	0.002			
−46	−1	_	1	13.76	13.76	0.000	0.85	0.53	91.09
	1	_	1	14.00	14.00	0.003			
	2	_	0	14.72	14.72	0.002			

[a] Standard uncertainties u are u(T) = 1 °C, $u_r(q_{Obs}) = u(q_{Obs})/\ u|q_{Obs}| = 0.02$ and u(P) = 0.03 MPa.

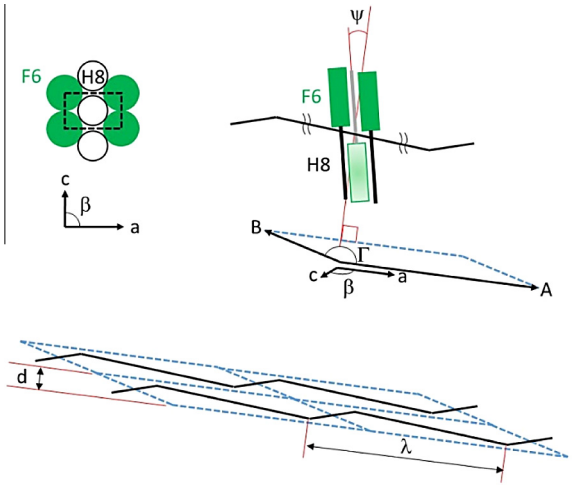

Fig. 11. Crystal structure and lattice for the postulated F6H8 ripple phase. Lattice parameters a, c, β, and A, B, Γ are provided in Tables 2 and 3, respectively. d is the layer spacing and ψ is the tilting angle of the F6H8 molecule vs. the normal to the A-axis.

measurements performed at −14 °C. However due to difficulties to measure at such low temperatures it might be possible that the F6H8 sample was not fully below the minor transition point. Furthermore, SFAs like F8H10 tend to supercool and form a metastable phase [10]. Nevertheless, a small decrease in the lattice parameters for the monoclinic sub cell could be observed when lowering the temperature down to −46 °C, while no change was observed in the long range order (Table 3). The minor transition could be the onset of rotational motions which would give rise to looser packing above the transition point.

SWAXD measurements were also performed on mixtures of F6H8 and C14 at −14 °C, Fig. 12. F6H8 and C14 crystals are in equilibrium with each other in mixtures at −14 °C. All Bragg peaks belong to either C14 crystals or F6H8 crystals and the intensity for the C14 peaks decreases with decreased C14 content. However the two phases do affect each other. This can be seen in supporting information Fig. S2 where the intensities of peaks originating from the pure F6H8-phase and the pure C14-phase are shown. The intensity of the F6H8 peak is significantly reduced already after addition of C14 to a weight fraction of 0.1, and shows that the pure F6H8-phase is very sensitive to C14. The C14-phase is less affected

Table 3
Observed and calculated peak positions (q_{Obs} and q_{Calc}) together with corresponding lattice parameters (A, B and Γ) and the miller indexes (h, k, l) and calculated densities (ρ) for the ripple F6H8 phase measured at two temperatures (T), −14 °C and −46 °C, respectively measured at a pressure (P) of 0.1 MPa.[a]

T/°C	*h*	*k*	*l*	q_{Obs}/nm^{-1}	q_{Calc}/nm^{-1}	Δq/nm^{-1}	*A*/nm	*B*/nm	*Γ*/°	*ρ*/g cm^{-3}
−14	1	0	_	3.10	3.10	0.000	9.42	4.64	167.6	1.558
	−1	1	_	3.33	3.33	0.000				
	0	1	_	6.29	6.29	0.000				
	2	0	_	6.22	6.20	0.020				
	−2	2	_	6.52	6.66	0.140				
	1	1	_	9.39	9.34	0.049				
	−1	2	_	9.62	9.58	0.044				
	0	2	_	12.54	12.58	0.040				
−46	1	0	_	3.10	3.10	0.000	9.42	4.64	167.6	1.587
	−1	1	_	3.33	3.33	0.000				
	0	1	_	6.29	6.29	0.000				
	2	0	_	6.22	6.20	0.020				
	−2	2	_	6.52	6.66	0.140				
	1	1	_	9.39	9.34	0.049				
	−1	2	_	9.62	9.58	0.044				
	0	2	_	12.54	12.58	0.040				

[a] Standard uncertainties u are u(T) = 1 °C, u(ρ) = 0.054 g cm^{-3}, $u_r(q_{Obs}) = u(q_{Obs})/ u|q_{Obs}| = 0.02$ and u(P) = 0.03 MPa.

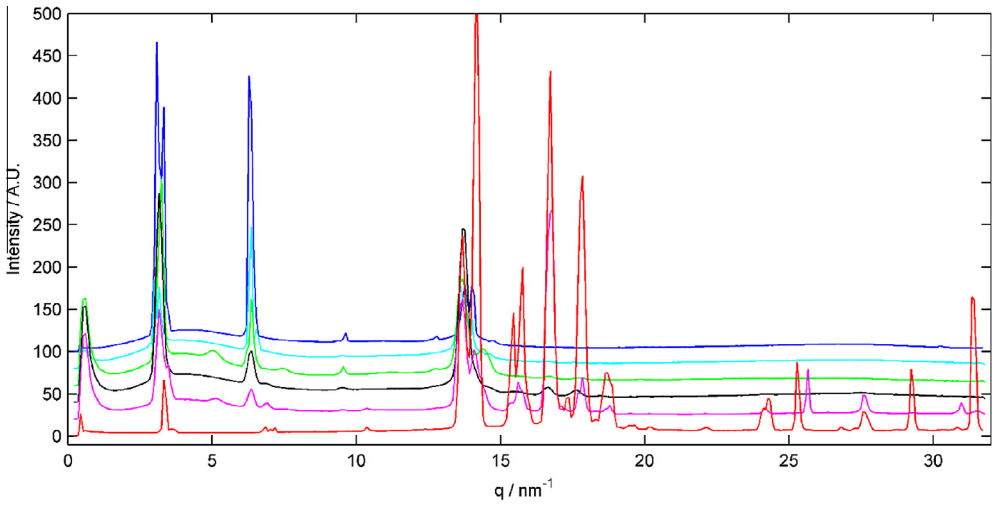

Fig. 12. X-ray diffractograms from mixtures of F6H8 and C14 at −14 °C. Measurements corresponding to decreasing weight fractions of F6H8, 1 (blue), 0.99 (cyan), 0.95 (green), 0.90 (black), 0.50 (magenta) and 0 (red), are shown from the top and down. (For interpretation of the references to colour in this figure legend, the reader is referred to the web version of this article.)

by addition of F6H8. The asymmetry of the system is also in agreement with observed asymmetry in Gibbs energy (Fig. 5B) and activity (Fig. 4A) of the fluid phase. The fact that no changes in peak positions for C14 are visible and that the decrease in peak intensity is linear with decreased amount of C14 indicates that no solid solution of F6H8 in C14 is formed. However, the nonlinear decrease in peak intensity for F6H8 shows that a solid solution of C14 in F6H8 might be formed. Nevertheless, we only use the activities for C14 when calculating the activity coefficients and Gibbs energy and hence these calculations are not affected by formation of solid solutions.

4. Conclusions

We conclude that pure C14 has one solid-liquid transition at 5.9 °C (ΔH = 48.0 kJ/mol), in accordance with previous studies. F6H8 displays two transitions, one minor at −42.3 °C (ΔH = 1.0 kJ/mol) and one major at −5.9 °C (ΔH = 16.6 kJ/mol). The minor transition likely corresponds to a solid-solid transition of F6H8 while the main transition corresponds to a solid-liquid transition. However, due to the low enthalpy of the main transition it is likely that F6H8 is not fully crystallized in the solid phase but partly amorphous. The data indicates that most probably the fluorinated segment is crystalline while the hydrogenated segment is amorphous. F6H8–C14 mixtures were found to display eutectic phase behavior with a eutectic point at −8.8 °C and a C14 weight fraction of 0.06. We determined the enthalpies of solution at infinite dilution and 25 °C to be 4.5 kJ/mol C14 in F6H8 and 6.5 kJ/mol F6H8 in C14. The asymmetry in the ITC measurements are in agreement with calculated activity coefficients and energy of mixing which also displayed an asymmetry with regard to composition. C14 crystalizes in a triclinic unit cell as shown before, whereas crystallization of F6H8 in a lamellar ripple phase is shown for the first time. This ripple phase comprises a bilayer of tilted alternating heavily interdigitated F6H8 molecules in an oblique subunit cell.

Acknowledgements

The MAX IV laboratory in Lund (Sweden) is acknowledged for providing time to run SAXS experiments. Authors are grateful to Prof. Ulf Olsson (Lund University) for valuable discussions and to Drs. Tomas Plivelic and Sylvio Haas (MAX-lab) and Dr. Marc Obiols Rabasda (Lund University) for technical support. This study was conducted as a joint research project, funded by Novaliq Gmbh, Heidelberg, Germany.

Appendix A. Supplementary data

Supplementary data associated with this article can be found, in the online version, at http://dx.doi.org/10.1016/j.jct.2016.10.032.

References

[1] M.P. Krafft, J.G. Riess, Chem Rev 109 (2009) 1741–1792.
[2] G. Gaines L, Langmuir 7 (1991) 3054–3056.
[3] M. Broniatowski, P. Dynarowicz-Łątka, W. Witko, J Fluorine Chem 126 (2005) 79–86.
[4] P. Lo Nostro, S. Ched, J Phys Chem 97 (1993) 6535–6540.
[5] M. Napoli, J. Fluorine Chem. 79 (1996) 59–69.
[6] J.F. Rabolt, T.P. Russell, R.J. Twieg, J Macromol 17 (1984) 2786–2794.
[7] R.J. Twieg, T.P. Russell, R. Siemens, J.F. Rabolt, Macromolecules 18 (1985) 1361–1362.
[8] M. Broniatowski, P. Dynarowicz-Łątka, Adv Colloid Interface Sci 138 (2008) 63–83.
[9] C. Ku, P. Lo Nostro, S. Chen, J Phys Chem 101 (1997) 908–914.
[10] M. Broniatowski, P. Dynarowicz-Łątka, W. Witko, Mol Cryst Liq Cryst 460 (2006) 63–74.
[11] M. Fujiwara, K. Satoh, S. Kondo, S. Ujiie, Macromolecules 39 (2006) 5836–5842.
[12] S. Mita, M. Fujiwara, S. Kondo, Mol Cryst Q Crys. 330 (1999) 37–44.
[13] C. Tsagogiorgasa, T. Jungb, J. Krebsa, B. Theisingerd, G. Becke, B.A. Yard, M. Quintel, Int J Pharm 422 (2012) 194–201.
[14] H. Meinert, A. Knoblich, Biomat, Art Cells Immobilization Biotechnol 21 (1993) 583–595.
[15] Frédéric Gerber, Marie Pierre Krafft, Michel Goldmann, Philippe Fontaine, Artif. Cells Blood Substit. Immobil. Biotechnol. 35 (2007) 211–220.
[16] P. Morgado, H. Zhao, F.J. Blas, C. McCab, L.P.N. Rebelo, E.J.M. Filip, J Phys Chem 111 (2007) 2856–2863.
[17] C. Wetterqvist, D. Wong, R. Williams, T. Stappler, E. Herbert, S. Freeburn, Br J Ophthalmol 88 (2004) 692–696.
[18] J.M. Martinez-Reina, J.M. Ruiz-Moreno, J.M. Montero, J. Rueda Curr Eye Res 30 (2005) 773–779.
[19] M. Schmutz, B. Michels, P. Marie, M.P. Krafft, Langmuir 19 (2003) 4889–4894.
[20] A.J. Bron, J.M. Tiffanya, S.M. Gouveiaa, N. Yokoib, L.W. Voon, Exp Eye Res 78 (2004) 347–360.
[21] F.J. Holly, Exp Eye Res 15 (1973) 515–525.
[22] Y. Ohashi, M. Dogru, K. Tsubota, Clin Chim Acta 369 (2006) 17–28.
[23] A.H. Rantamäki, T. Seppänen-Laakso, M. Oresic, M.. Jauhiainen, J.M. Holopainen, PLoS One 6 (2011), e19553-e19553.
[24] I. Wadso, R.N. Goldberg, Pure Appl Chem 73 (2001) 1625–1639.
[25] A.R. Ubbelohde, Trans. Faraday Soc. 34 (1938) 0282–0299.
[26] W. Crawford, C.L.A. Harbourn, Anal Chem 27 (1955) 1449–1451.
[27] A. Liu, K. Pusicha, A.M. Demiriz, F. Kohler, J. Solution Chem. 20 (1991) 39–56.
[28] S. Landa, J. Romovacek, H. Romovackova, Collect Czech Chem Commun 20 (1955) 835–839.
[29] M.D. Tilicheev, V.P. Peshkov, S.A. Yuganova, Zh Obshch Khim 21 (1951) 1229–1237.
[30] E.S. Domalski, E.D. Hearing, J Phys Chem Ref Data 25 (1996) 1–525.
[31] H.L. Finke, M.E. Gross, G. Waddington, H.M. Huffman, J Am Chem Soc 76 (1954) 333–341.
[32] M. Yang, E. Terakawa, Y. Tanaka, T. Sotani, S. Matsuo, Fluid Phase Equilib 194 (2002) 1119–1129.
[33] G. Parks, D. Light, J Am Chem Soc 56 (1934) 1511–1513.
[34] C.P. Jariwala, L.J. Mathias, J Macromol 26 (1993) 5129–5136.
[35] T.P. Russell, J.F. Rabolt, R.J. Twieg, R.L. Siemens, Macromolecules 19 (1986) 1135–1143.
[36] J. Höpken, M. Möller, Macromolecules 25 (1992) 2482–2489.
[37] R. Holm, E.B. Jorgensen, M. Harborg, R. Larsen, P. Holm, A. Mullertz, J. Jacobsen, Eur J Pharm Sci 42 (2011) 416–422.
[38] J.G. Riess, M.P. Krafft, in: R.M. Winslow (Ed.), Blood Substitutes, Academic Press, London, 2006, pp. 254–275.
[39] H.W. Starkweather, Macromolecules 19 (1986) 1131–1134.
[40] G.T. Dee, B.B. Sauer, B.J. Haley, Macromolecules 27 (1994) 6106–6111.
[41] J. Visjager, T.A. Tervoort, P. Smith, Polymer 40 (1999) 4533–4542.
[42] I. Schröder, Zeitschrift f physik Chemie XI (1893) 449–465.
[43] J.M. Prausnitz, Adv Chem Eng 7 (1968) 139–206.
[44] A. Guinier, G. Fournet, Small-Angle Scattering of X-Rays, John Wiley & Sons, New York, 1955.
[45] S.C. Nyburg, F.H. Pickard, Acta Crystallogr Sec B 30 (1974) 1885–1886.
[46] N. Norman, H. Mathisen, Acta Chem Scand 26 (1972) 3913–3916.
[47] P. Marczuk, P. Lang, Macromolecules 31 (1998) 9013–9018.
[48] D.M. Small, in: D.J. Hanahan (Ed.), Handbook of lipid resarch volume 4 the physical chemistry of lipids: from alkanes to phospholipids, Plenum Press, New York, 1986, pp. 21–40.
[49] K. Larsson, Acta Chem Scand 20 (1966) 2255.

Supporting information

Interactions between Semifluorinated Alkanes and Alkanes: A Phase Study of the Perfluorohexyloctane and Tetradecane system.

Anna Runnsjö[a,b,*], Vitaly Kocherbitov [a,b], Gesche Graf[c], Anthony Pettigrew[c], Dieter Scherer[c], Kell Mortensen[d] and Johan Engblom[a,b]

[a] Biomedical Science, Faculty of Health and Society, Malmö University, SE-205 06 Malmö, Sweden
[b] Biofilms - Research Center for Biointerfaces, Malmö University, SE-205 06 Malmö, Sweden
[c] Novaliq GmbH, Im Neuenheimer Feld 515, D-69120 Heidelberg, Germany
[d] Niels Bohr Institute, University of Copenhagen, Universitetsparken 5, 2100 København Ø
* Corresponding author: anna.runnsjo@gmail.com

Table S1. Substance table

Chemical name	Source	*Initial mole fraction purity	Purification method	*Density at 20 °C /g mL^{-1}	*Refractive index at 20 °C
Perfluorohexyloctane	Novaliq GmBH	0.9988	none	1.331	1.343
Tetradecane	Sigma Aldrich	0.99	none	0.762	1.429

* As specified by the producer.

Table S2.
Experimental (solid + liquid) equilibrium temperatures T and liquid mole fractions x for the system tetradecane (C14) + perfluorohexyloctane (F6H8) at pressure P=0.1Mpa.[a]

wt% C14	x_{C14}	T/°C	Solid phase
0	0.000	-5.9	F6H8
1.0	0.022	-6.1	F6H8
2.1	0.045	-6.8	F6H8
3.1	0.064	-7.2	F6H8
4.0	0.083	-8.1	F6H8
4.9	0.102	-8.0	C14
6.3	0.128	-5.3	C14
8.3	0.165	-3.4	C14
10.0	0.195	-2.0	C14
20.0	0.353	1.4	C14
30.0	0.483	3.1	C14

50.0	0.685	4.1	C14
66.9	0.815	4.8	C14
90.0	0.952	6.1	C14
100.0	1.000	5.9	C14

[a] Standard uncertainties u are u(T) = 0.6 °C , u(x) = 0.001 and u(P)= 0.02 MPa.

Table S3.
Experimental eutectic temperatures T and mole fractions x for the system tetradecane (C14) + perfluorohexyloctane (F6H8) at pressure P = 0.1 MPa.[a]

wt% C14	**x_{C14}**	**T /°C**
0	0.000	
1.0	0.022	-9.4
2.1	0.045	-8.8
3.1	0.064	-8.6
4.0	0.083	-8.7
4.9	0.102	-8.5
6.3	0.128	-8.6
8.3	0.165	-8.7
10.0	0.195	-8.8
20.0	0.353	-8.7
30.0	0.483	-8.8
50.0	0.685	-9.1
66.9	0.815	-9.5
90.0	0.952	-11.2
100.0	1.000	

[a] Standard uncertainties u are u(T) = 0.7 °C , u(x) = 0.001 and u(P) = 0.02 MPa.

Table S4. Experimental temperature measured for the solid-solid transition of F6H8 at pressure P = 0.1 MPa.[a]

wt% C14	**x_{C14}**	**T /°C**
0	0.000	-42.3
1.0	0.022	-43.2
2.1	0.045	-44.3
3.1	0.064	-45.8
4.0	0.083	-46.3
4.9	0.102	-46.7
6.3	0.128	-46.5
8.3	0.165	-47.9
10.0	0.195	-46.9
20.0	0.353	-45.5
30.0	0.483	-47.1
50.0	0.685	-47.2
66.9	0.815	-46.8
90.0	0.952	-47.6
100.0	1.000	

[a] Standard uncertainties u are u(T) = 1 °C , u(x) = 0.001 and u(P) = 0.03 MPa.

F6H8

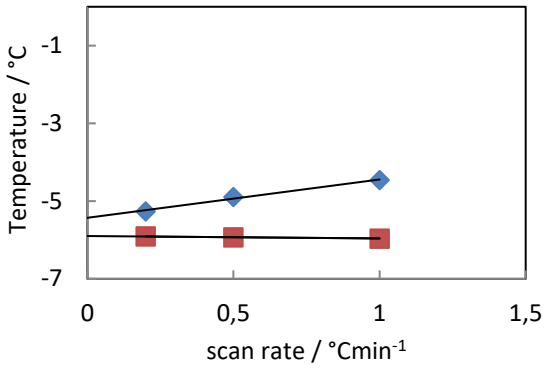

C14

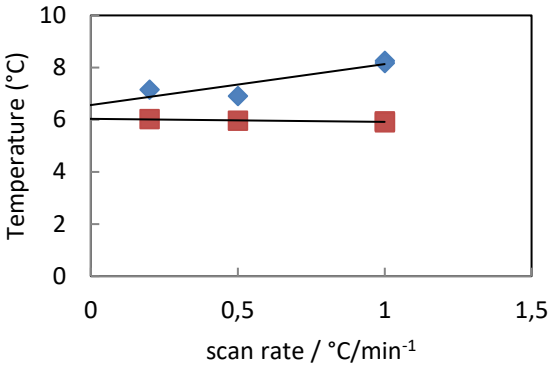

99% F6H8

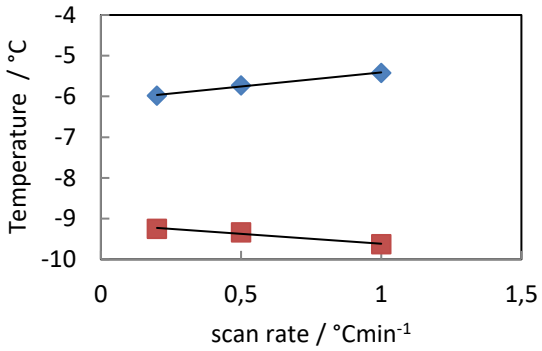

98% F6H8

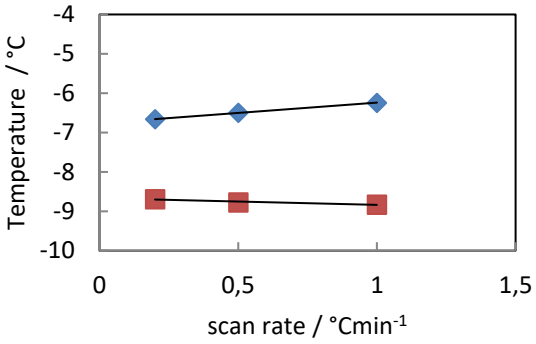

97% F6H8

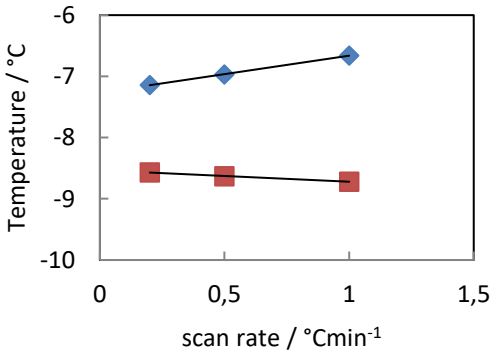

95% F6H8

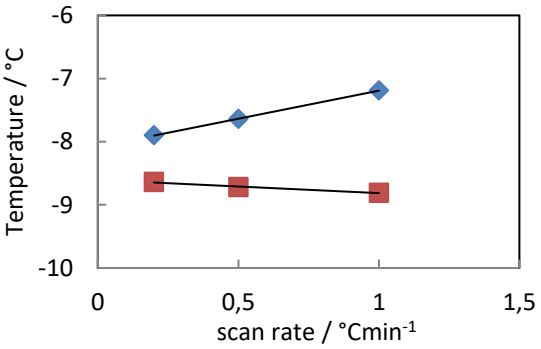

94% F6H8

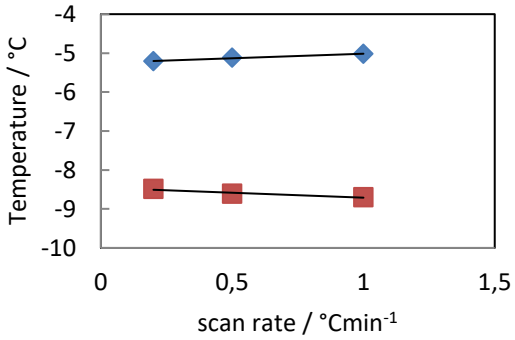

92% F6H8

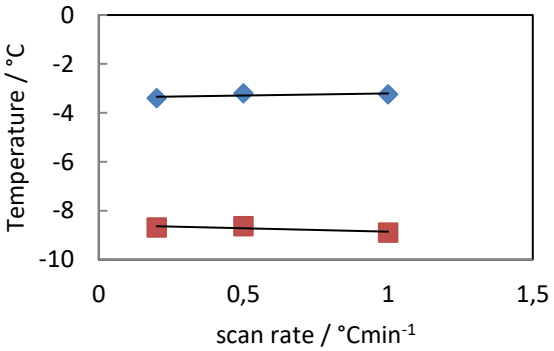

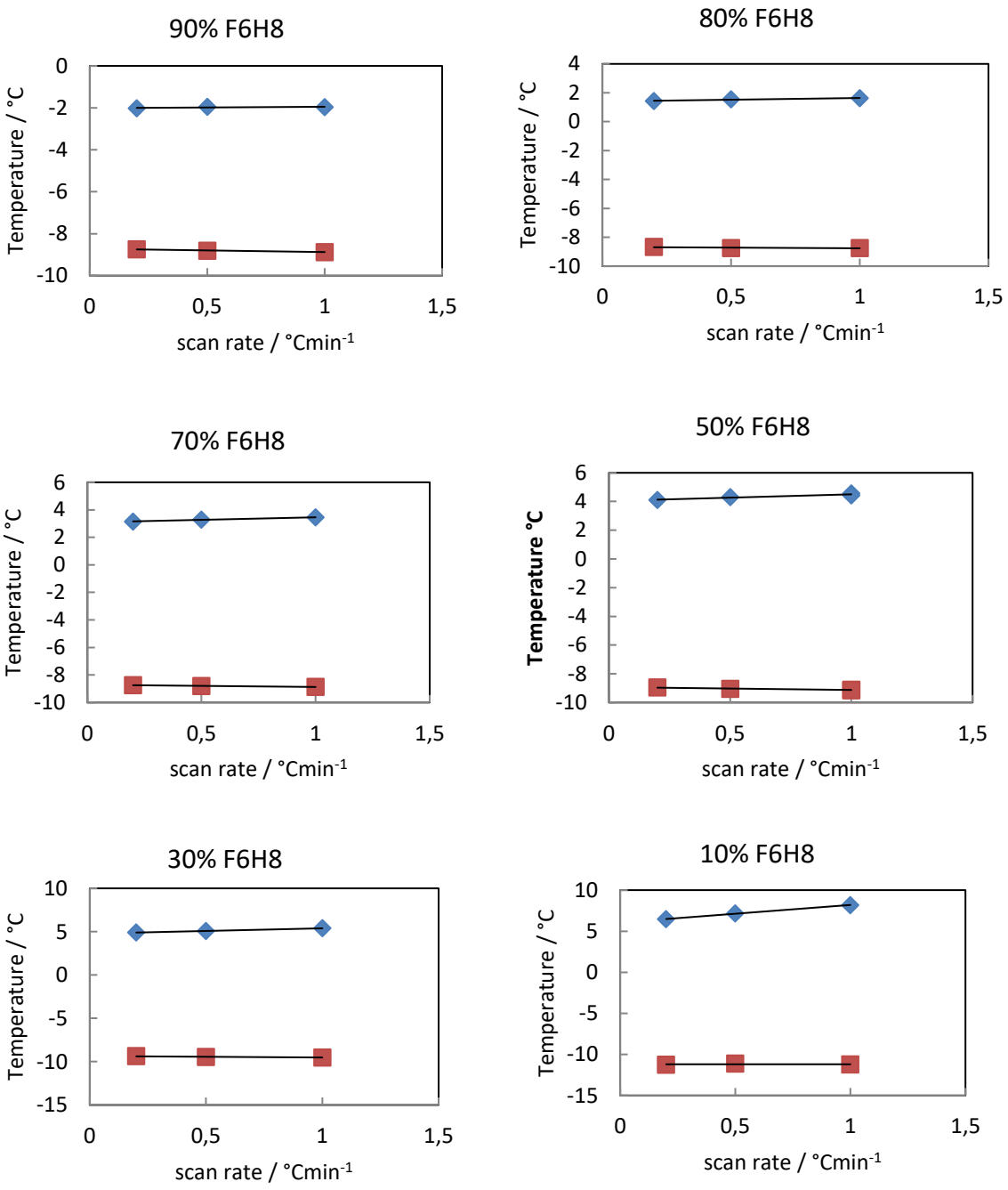

Figure S1. Transition endset (blue diamonds) and onset temperatures (red squares) for F6H8 and C14 obtained with DSC using heating rates of 1, 0.5 and 0.2 °C/min. Endset temperatures decrease linearly with decreased heating rate, while the onset temperatures remain constant. Extrapolation to 0 °C/min heating rate, using a linear fit, were hence used to determine endset of transition points.

Table S5. Experimental enthalpy of solution for titration of F6H8 into C14 at pressure p = 0.1 MPa and temperature T=25 °C.[a]

Injection number	**Final mixture composition (F6H8/C14) after injection /molkg^{-1}**	**ΔH /kJmol^{-1}**
1	0.012	6.49
2	0.024	6.42
3	0.037	6.40
4	0.049	6.45
5	0.062	6.35
6	0.073	6.37
7	0.085	6.29
8	0.098	6.25

[a] Standard uncertainties u are u(F6H8/C14) = 0.002 mol kg^{-1}, u(ΔH)=0.3 kJmol^{-1} , u(p) = 2 kPa and u(T) = 0.01 °C

Table S6. Experimental enthalpy of solution for titration of C14 into F6H8 at pressure p = 0.1 MPa and temperature T = 25 °C.[a]

Injection number	**Final mixture composition (C14/F6H8) after injection /molkg^{-1}**	**ΔH /kJmol^{-1}**
1	0.009	4.22
2	0.019	3.92
3	0.028	3.58
4	0.037	3.31
5	0.047	3.17
6	0.056	3.00
7	0.065	2.84
8	0.074	2.74

[a] Standard uncertainties u are u(C14/F6H8) = 0.003 mol kg^{-1}, u(ΔH)=0.2 kJmol^{-1}, u(p) = 2 kPa and u(T) = 0.01 °C

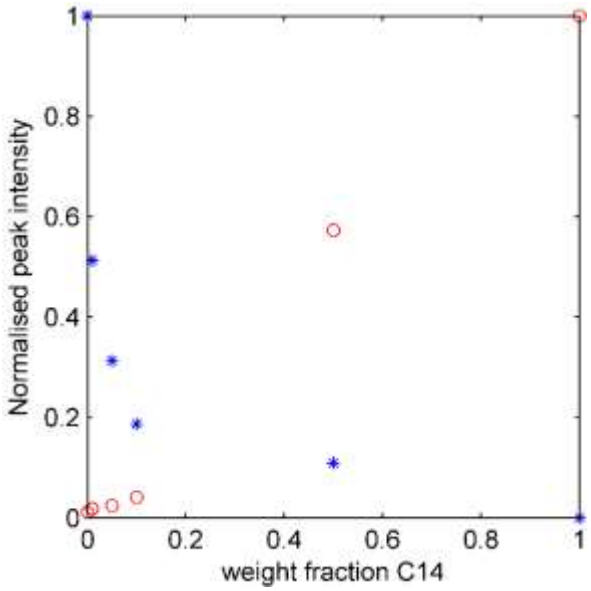

Figure S2. Normalized peak intensities measured by SWAXD for peaks representing pure C14 and F6H8. For F6H8 (blue stars) the peaks at q=6.3 nm^{-1} were used and for C14 (red circles) the peaks at q=16.7 nm^{-1} were used.